ELSEVIER

Physica C 279 (1997) 1–10

PHYSICA C

Structure and superconductivity in Cr-substituted $HgBa_2CuO_{4+\delta}$

O. Chmaissem [a,*], J.D. Jorgensen [b], D.G. Hinks [b], B.G. Storey [c], B. Dabrowski [d], H. Zhang [c], L.D. Marks [c]

[a] *Science and Technology Center for Superconductivity, Argonne National Laboratory, Argonne, IL 60439, USA*
[b] *Materials Science Division, Argonne National Laboratory, Argonne, IL 60439, USA*
[c] *Department of Materials Science and Engineering and Science and Technology Center for Superconductivity, Northwestern University, Evanston, IL 60208, USA*
[d] *Physics Department, Northern Illinois University, Dekalb, IL 60115, USA*

Received 28 January 1997; revised 27 March 1997

Abstract

Chromium-substituted $Hg_{1-x}Cr_xBa_2CuO_{4+\delta}$ compounds have been synthesized. Cr can be incorporated into the structure with a solubility limit around $x \approx 0.27$. Cr substitutes at the Hg site and is tetrahedrally coordinated to four oxygen atoms. Two of these are apical oxygen atoms that have moved to new positions (O2′) and two are in the Hg/Cr plane (O3) at a (x x 0) site. Additional oxygen atoms (O4) in the Hg/Cr plane at (1/2 1/2 0) affect the carrier concentration, as for $HgBa_2CuO_{4+\delta}$. In the as-synthesized samples, T_c decreases with increasing Cr content. Attempts to adjust the carrier concentration by post annealing in oxygen at low temperature destroy superconductivity because the samples are metastable under ambient conditions. © 1997 Elsevier Science B.V.

Keywords: Mercury-based superconductors; Chromium substitution; Superconductivity; Neutron diffraction; Structural analysis

1. Introduction

Chemical instability during synthesis and the relatively poor flux pinning properties are limiting the use of Hg–Ba–Ca–Cu–O superconducting compounds in technological applications. Cationic substitutions have been explored as a means of simplifying and stabilizing the synthesis chemistry and enhancing the flux pinning properties. Many substituents are found to replace, either partially or totally, the Hg, Ba or Ca [1–7] and there are claims of improved chemical stability and flux pinning [3,8,9]. The present work on Cr-substituted compounds is part of our effort to find substituents that can enhance the flux pinning while not degrading the high T_c. In previous papers [10,11], we reported on the possible relationship between the crystal structure and enhanced flux pinning in Cr- and Re-substituted Hg-based superconductors where Ba is replaced by Sr. In those compounds, only Cr concentrations near the solubility limit (where half of the Hg is substituted by Cr) can be formed. To properly explore the effect of Cr substitution on properties, compounds that form a continuous solid solution extending to zero Cr content are desired. In the present paper, we report the synthesis and properties of a series of Cr-substituted Ba-containing samples, namely $Hg_{1-x}Cr_xBa_2Cu$-

* Corresponding author. Tel.: +1 630 2525541; fax: +1 630 2527777.

PII S0921-4534(97)00134-2

$O_{4+\delta}$, where the Cr content can be continuously varied from $x = 0$ to ~ 0.27.

The crystal structures of the parent compounds $HgBa_2Ca_{n-1}Cu_nO_{2n+2+\delta}$ (hereafter denoted as Hg-1201, Hg-1212 and Hg-1223 for the $n = 1$, 2 and 3 compounds, respectively) have been studied in detail [12–19]. The structural studies suggest that interstitial oxygen atoms, O_δ (located in the center of the Hg layer), are the dominant doping mechanism for superconductivity. T_c can be varied over a wide range by changing the oxygen content in this crystallographic site. The origin of hole doping becomes less obvious when cationic substitutions are present. The reported Hg-site substituents (e.g. Mo, V, Re, Tl, Pb, Cr, etc.) generally require oxygen configurations different from the 'dumbbell' configuration characteristic of divalent Hg atoms in this structure. At high concentrations of the substituting cations, the interstitial oxygen site normally used to control the carrier concentration is 'blocked' by oxygen atoms bonded to the cation substitutional defect. Thus, another reason for studying cation substitutions in low concentrations is to attempt to retain a variable oxygen doping mechanism. The compounds studied here are able to incorporate oxygen in the interstitial site, which, in principle, provides a method for adjusting the carrier concentration. However, the samples are found to be metastable in other than the synthesis conditions. When oxygen anneals are performed at lower temperatures to adjust the oxygen content, the samples phase separate to a phase with near zero Cr content and a phase with high Cr content which subsequently decomposes.

2. Synthesis and characterization

Samples of nominal composition $Hg_{1-x}Cr_xBa_2CuO_{4+\delta}$ ($0 \leq x \leq 0.4$) were prepared in sealed quartz tubes. In a first step, Ba_2CuO_z precursors were obtained by heating a stoichiometric mixture of $Ba(NO_3)_2$ and CuO in flowing oxygen gas at $\cong$ 600°C (6 h) and 860°C (18–20 h). The heating step at $\cong$ 600°C was necessary to avoid melting with resultant phase separation of the mixture. The melting point of the mixture decreases significantly with the addition of Cr_2O_3 and it becomes quite difficult to contain the mixture. Subsequently, appropriate amounts of Cr_2O_3 were added to the pre-reacted Ba_2CuO_z powder and fired at 860°C for 15–20 h. With this process we were able to obtain good quality precursors that were black in color for low Cr

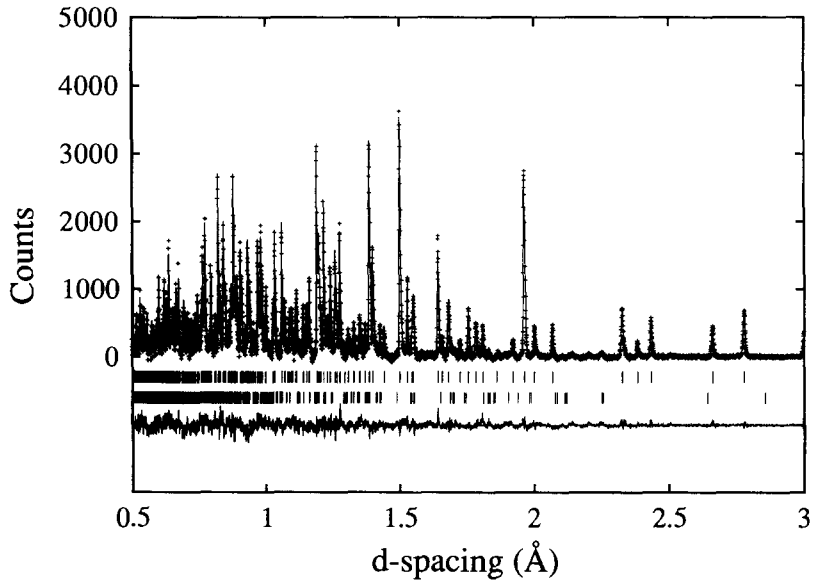

Fig. 1. Best-fit Rietveld refinement profile showing observed (+) and calculated (line) intensities. The markers below the profile correspond to Bragg peak positions for $Hg_{0.88}Cr_{0.09}Ba_2CuO_{4+\delta}$ (top) and $Ba_2Cu_3O_{5+\delta}$ (bottom). The difference between observed and calculated values is shown at the bottom. The refined background was subtracted from the profile.

Table 1
Refined structural parameters for $Hg_{1-x}Cr_xBa_2CuO_{4+\delta}$ using the tetragonal space group P4/mmm

x	(nominal)	0	0.1	0.2	0.3	0.4
Hg	at (0 0 0)					
	B (Å^2)	1.02(4)	0.88(5)	1.41(5)	0.82(6)	0.95(7)
	n	0.966(6)	0.822(8)	0.706(8)	0.633(7)	0.635(9)
Cr	at (x 0 0)					
	x		0.11(4)	0.13(1)	0.10(1)	0.12(1)
	B (Å^2)		0.88(5)	1.41(5)	0.82(6)	0.95(7)
	n		0.088(8)	0.228(4)	0.284(8)	0.284(8)
Ba	at (1/2 1/2 z)					
	z	0.2997(2)	0.2993(2)	0.2979(2)	0.2976(2)	0.2975(2)
	B (Å^2)	0.67(3)	0.68(4)	0.65(4)	0.59(4)	0.59(4)
	n	2	2	2	2	2
Cu	at (0 0 1/2)					
	$100 \times U_{11}$	0.40(3)	0.12(6)	0.77(5)	0.26(6)	0.32(7)
	$100 \times U_{22}$		0.12(6)	0.77(5)	0.26(6)	0.32(7)
	$100 \times U_{33}$		1.5(1)	1.9(1)	0.7(1)	1.0(1)
	n	1	1	1	1	1
O1	at (1/2 0 1/2)					
	$100 \times U_{11}$	0.64(3)	0.40(9)	1.06(7)	0.36(9)	0.16(9)
	$100 \times U_{22}$		0.64(9)	1.15(7)	0.32(8)	0.46(9)
	$100 \times U_{33}$		1.5(1)	1.87(9)	1.5(1)	1.8(1)
	n	2	2	2	2	2
O2	at (0 0 z)					
	z	0.2072(2)	0.2080(3)	0.2126(3)	0.2133(4)	0.2130(5)
	B (Å^2)	1.20(3)	1.17(5)	1.45(5)	1.09(7)	1.25(7)
	n	2	1.82(1)	1.51(1)	1.43(1)	1.43(1)
O2′	at (x 0 z)					
	x		0.14(1)	0.093(3)	0.100(3)	0.100(3)
	z		0.159(5)	0.156(2)	0.152(2)	0.149(2)
	B (Å^2)		1.17(5)	1.45(5)	1.09(7)	1.25(7)
	n		0.18(2)	0.46(1)	0.57(1)	0.57(1)
O3	at (x x 0)					
	x		0.355(6)	0.369(2)	0.362(2)	0.363(2)
	B (Å^2)		0.8	0.8	0.8	0.8
	n		0.18(2)	0.46(1)	0.57(1)	0.57(1)
O4	at (1/2 1/2 0)					
	B (Å^2)	0.8	0.8	0.8	0.8	0.8
	n	0.139(5)	0.087(9)	0.066(7)	0.061(9)	0.064(9)
a (Å)		3.88407(3)	3.90671(4)	3.92575(3)	3.93882(4)	3.94066(4)
c (Å)		9.5425(1)	9.4237(2)	9.3049(2)	9.2500(2)	9.2400(2)
R_p (%)		2.47	3.42	3.22	3.02	3.12
R_{wp} (%)		3.76	5.21	4.96	4.68	4.84
χ^2		2.224	1.702	2.019	1.639	1.693

Constraints are: U(Hg) = U(Cr), U(O2) = U(O2′), n(O2) + n(O2′) = 2, 2 × n(Cr) = n(O2′) = n(O3).

concentrations and dark-greenish black for higher Cr concentrations ($x \geq 0.3$). Stoichiometric amounts of HgO were then mixed with the resultant precursor and the mixture was pelletized, sealed in evacuated quartz tubes, and fired at 800°C for 6 h. The approximate tube dimensions were 8 mm I.D., 12 mm O.D. and 8–9 cm long. Heating and cooling rates were about 3.5°C/min.

The samples were characterized using a Rigaku Dmax X-ray diffractometer (Cu Kα wavelength), DC resistance and AC susceptibility measurements. Neutron powder diffraction measurements were performed on the special environment powder diffractometer (SEPD) [20] at Argonne's intense pulsed neutron source (IPNS). Data were collected for 8–10 h for ~2g samples. Transmission electron microscopy (TEM) and the energy dispersive spectroscopy (EDS) technique were used to investigate the chemical compositions of the samples. Preliminary neutron analysis showed minute traces of $Ba_2Cu_3O_{5+\delta}$ ($\approx$ 4–6%) in the $x \leq 0.2$ samples while $HgBaO_2$ and CuO were identified in the $x >$ 0.2 samples (up to 10%). Additional weak impurity lines that belong to a Ba and Cr rich phase (possibly $BaCrO_4$) are also seen.

3. Structure — neutron powder diffraction

The neutron powder diffraction data were refined by the Rietveld technique using the GSAS code [21] over a d-spacing range of 0.5–4 Å, which included ~1281 Bragg peaks. The starting model used the structural parameters of the $HgBa_2CuO_{4+\delta}$ compound [12,13] (tetragonal space group P4/mmm) but with the Cr defect and its associated oxygen atoms as were previously refined for the $Hg_{1-x}Cr_xSr_2CuO_{4+\delta}$ compound [10]. The identified impurity phases were included in the refinements and an exponential pseudovoight function and cosine Fourier series were used to describe the peak profile and the background, respectively. Successful refinements were achieved for all samples. Fig. 1 shows the data and best-fit Rietveld profile for the sample with $x = 0.2$ starting composition. Refined structural parameters and selected bond-lengths are given in Tables 1 and 2, respectively.

Cr atoms substitute at the Hg sites but are displaced in the x-direction to allow a tetrahedral coordination with four neighboring oxygen atoms. Two of these are provided by part of the apical oxygen atoms O2′ which are also displaced in the x-direc-

Table 2
Selected atom–atom distances (Å) for $Hg_{1-x}Cr_xBa_2CuO_{4+\delta}$

x (nominal)	0	0.1	0.2	0.3	0.4
Hg–Cr [a]		0.42(15)	0.51(5)	0.39(5)	0.47(5)
Hg–O2	1.974(1)	1.960(3)	1.978(3)	1.973(4)	1.968(4)
Hg–O4	2.74646(2)	2.76246(3)	2.77592(2)	2.78517(3)	2.78647(3)
Cr–O2′		1.77(9)	1.70(3)	1.61(3)	1.63(3)
Cr–O3		1.69(9)	1.73(3)	1.76(3)	1.72(2)
Ba–O1	2.725(1)	2.719(1)	2.718(1)	2.717(1)	2.717(1)
Ba–O2	2.8855(7)	2.894(1)	2.887(1)	2.892(1)	2.894(1)
Ba–O2′		2.76(3)/3.42((4)	2.853(7)/3.32(1)	2.857(8)/3.36(1)	2.872(9)/3.37(1)
Ba–O3		2.932(9)	2.867(3)	2.858(3)	2.853(4)
Ba–O4	2.859(1)	2.821(2)	2.772(2)	2.753(2)	2.749(2)
Cu–O1	1.94204(1)	1.95336(2)	1.96287(2)	1.96941(2)	1.97033(2)
Cu–O2	2.797(1)	2.752(3)	2.674(3)	2.652(4)	2.652(4)
Cu–O2′		3.25(5)	3.22(2)	3.24(1)	3.27(2)
Angles:					
O2′–Cr–O2′		116.0(9)	117.8(3)	121.6(3)	115.6(3)
O2′–Cr–O3		107.8(8)	106.3(2)	106.7(4)	107.2(3)
O3–Cr–O3		110.0(9)	114.1(3)	108.1(3)	112.5(3)

[a] No Hg–Cr distances actually exist. This is the magnitude of the displacement of Cr off the normal Hg site.

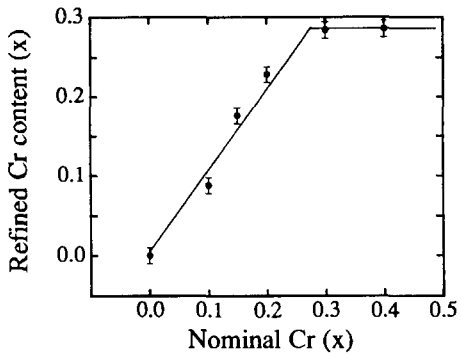

Fig. 2. Cr content in the $Hg_{1-x}Cr_xBa_2CuO_{4+\delta}$ phase determined by Rietveld refinement as a function of Cr starting composition. These data indicate a solubility limit at $x \approx 0.27$.

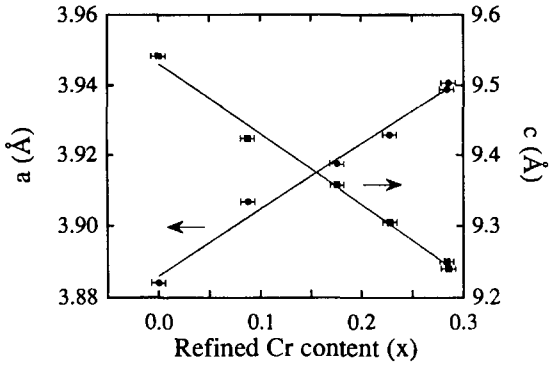

Fig. 3. Lattice parameters a and c as a function of Cr content determined by Rietveld refinement.

tion but in the opposite direction. The other two oxygen atoms are provided by the in-plane O3 atoms. In the refinements, n(O2′) is constrained to be equal to n(O3), and these oxygen contents are constrained to be twice the refined Cr content [n(Cr)]. These constraints are consistent with an assumption of isolated CrO_4 units (i.e. no Cr clustering) and result in a more accurate refinement of the Cr content. The displacements of the Cr, O2′ and O3 atoms are necessary to achieve appropriate bond lengths between Cr atoms and their oxygen neighbors. Nearly perfect tetrahedra are formed in all the samples. The three tetrahedral angles are found to be in the order of 106–118° and are comparable to those found in the literature for Cr atoms in a similar configuration (Table 2).

The refined Cr contents show that a Cr solubility limit (for this synthesis procedure) is reached at about $x \sim 0.27$. This is most clear when the refined Cr content is plotted vs. the starting composition, as shown in Fig. 2. EDS analyses were employed to provide an additional measure of the cationic compositions of the samples. Electron diffraction mode (TEM) was used to positively identify the (Hg, Cr)-1201 crystallites and a statistical analysis was performed on about twenty crystals for each sample. Table 3 lists the site occupancies for Hg and Cr obtained by Rietveld refinement and the corresponding cation ratios as determined by EDS. The total Hg + Cr compositions determined by EDS and Rietveld refinement agree to within 0.04 in the worst case, and there is also good agreement for the Cr:Hg ratios determined by the two methods. Hereafter, the Cr contents discussed in this paper will be those determined by Rietveld refinement. The lattice parameters are found to depend on the Cr content with a increasing linearly from 3.8841 Å to 3.9407 Å and c decreasing linearly from 9.5425 Å to 9.2400 Å with increasing x, as shown in Fig. 3. These monotonic variations indicate that Cr is incorporated as a continuous solid solution extending from $x = 0$. This is in contrast to the $Hg_{1-x}Cr_xSr_2CuO_{4+\delta}$ compounds, where only $x \sim 0.5$ can be formed [10].

Table 3
Hg and Cr occupancies for $Hg_{1-x}Cr_xBa_2CuO_{4+\delta}$ (nominal $x = 0$–0.4 starting compositions) as determined by Rietveld refinements and EDS chemical analysis

x	0.0		0.10		0.15		0.20		0.30		0.40	
	EDS	neutron	EDS	neutron	EDS	neutron	EDS	neutron	EDS	neutron	EDS	neutron
Cr	0	0	0.12(1)	0.09(1)	0.18(1)	0.16(1)	0.21(1)	0.23(1)	0.24(1)	0.28(1)	0.25(1)	0.28(1)
Hg	1.01(1)	0.97(1)	0.83(1)	0.82(1)	0.73(1)	0.75(1)	0.71(1)	0.71(1)	0.66(1)	0.63(1)	0.66(1)	0.64(1)
Hg + Cr	1.01(1)	0.97(1)	0.95(2)	0.91(2)	0.91(2)	0.91(2)	0.92(2)	0.94(2)	0.90(2)	0.92(1)	0.91(1)	0.92(1)

The values are normalized to 2 Ba atoms per unit cell.

Cr atoms, when incorporated into the structure of Sr-based Hg-1201, are found to order and cluster in a large supercell of approximate dimensions $5a \times 5a \times 2c$ [10]. In the present work, such a supercell was not observed in any of the $Hg_{1-x}Cr_xBa_2CuO_{4+\delta}$ samples. TEM selected area diffraction patterns show only the regular tetragonal pattern without any extra diffraction spots or streaking. These observations support our assumption that Cr atoms are randomly dispersed on the Hg sites in the present samples. A logical explanation for this is that the lower concentration of Cr in the present samples does not require ordering as is the case when the maximum allowed Cr solubility limit is approached in the Sr-substituted compounds [10]. The maximum allowed solubility limit is $x = 0.5$ because at this concentration the O3 oxygen atoms associated with the Cr defects occupy all available oxygen sites in the Hg/Cr plane [10]. When this maximum allowed Cr content is approached, the Cr defects order to form the supercell because of limitations on how the CrO_4 units must be oriented in order to achieve the maximum concentration [10].

Because Cr atoms randomly occupy the Hg sites, the CuO_2 plane experiences different local environments. Displacements of Cu atoms and O1 oxygen atoms along the c-axis could occur as a result of the asymmetry of the (Hg,Cr) layers directly above and below. However, the magnitudes of these displacements are small (estimated to be less than 0.2 Å). For this reason, these atoms were assigned anisotropic temperature factors. The refined temperature factors do indeed show unusually large components in the z-direction.

Cr substitution systematically shortens the blocking layer (which is simply the c-axis length for compounds with one CuO_2 layer). The c-axis decreases 0.30 Å upon going from $x = 0.0$ to maximum Cr content ($x \approx 0.27$). This shortening results almost entirely from a shortening of the Cu–O2 apical bond length, as shown in Fig. 4, which is a direct consequence of the Cr substitution as will be discussed in the next paragraph. When this behavior is extrapolated to $x = 0.5$ (the nominal Cr concentration achieved in $Hg_{1-x}Cr_xSr_2CuO_{4+\delta}$ compounds) both the c-axis and the Cu–O2 bond length would be significantly longer in the present compounds than in those where Sr has been substituted for Ba. (For

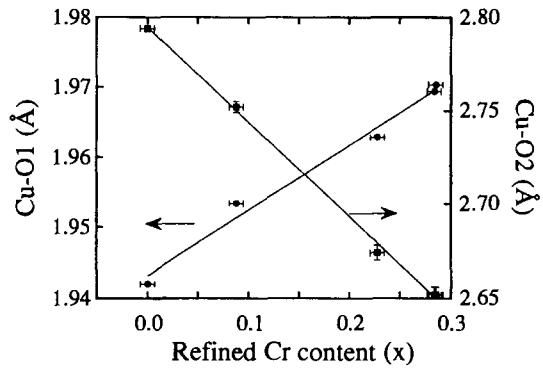

Fig. 4. Cu–O distances as a function of Cr content (x), for $Hg_{1-x}Cr_xBa_2CuO_{4+\delta}$.

$Hg_{1-x}Cr_xSr_2CuO_{4+\delta}$, $c = 8.696$ Å and (Cu–O2) = 2.25 Å [10]). This is as expected, based on the smaller ionic size of Sr compared to Ba. The in-plane Cu–O1 bond is lengthened by the addition of Cr (Fig. 4) thus reflecting the change in carrier concentration.

The apical oxygen atom (O2′) that becomes bonded to Cr is pulled away from the Cu atom. The Cu–O2′ distance is 3.25 Å (within one standard deviation) for all Cr concentrations. This oxygen atom has essentially been removed from the coordination shell of the Cu atom, leaving Cu with five oxygen neighbors in pyramidal coordination rather than six oxygen neighbors in octahedral coordination. However, in an attempt to establish a more sensible bond length with O2′, Cu atoms would move closer to the Hg layer. This would result in a shorter Cu–Hg average distance with elongated thermal ellipsoids (see Table 1). As the Hg–O2 distance is well defined and has very little variability the consequence is a shorter average Cu–O2 distance. Because of the effect of Cr on the structure, we have previously speculated that Cr defects were unlikely to form both above and below the same Cu atom, because of four-coordinated copper being energetically unfavorable compared to the other configurations.

4. Superconducting properties

The results of AC susceptibility measurements are shown in Fig. 5. T_c decreases with increasing Cr

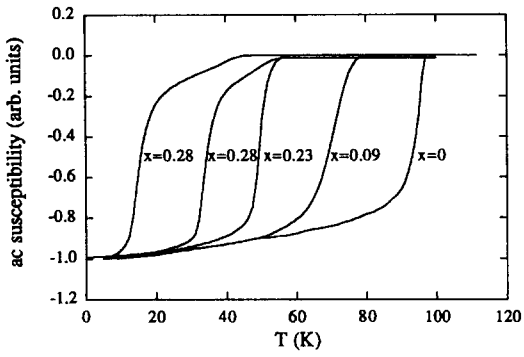

Fig. 5. AC magnetic susceptibility for $Hg_{1-x}Cr_xBa_2CuO_{4+\delta}$.

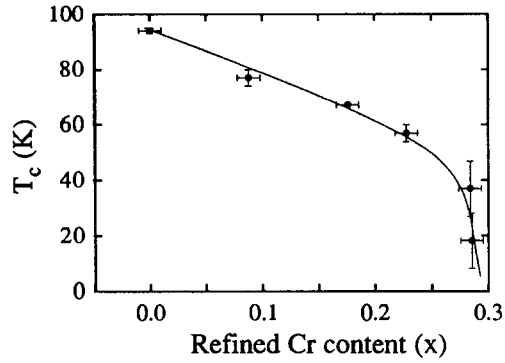

Fig. 6. T_c as a function of refined Cr content, x, for $Hg_{1-x}Cr_xBa_2CuO_{4+\delta}$.

content. Sharp transitions are obtained for the samples with $x = 0$, 0.09 and 0.23. Broad transitions, with a shape suggesting two-phase behavior rather than a continuous distribution of composition, are observed for the two samples with starting compositions beyond the solubility limit. A possible explanation for this behavior will be discussed later. A plot of T_c vs. Cr content is shown in Fig. 6. The typical inverse parabolic relationship between T_c and the chemical variable that controls the carrier concentration is observed. Although the refinement of neutron diffraction data shows no difference in Cr content (within the error bars) for the samples with 0.3 and 0.4 Cr starting compositions, T_c values are slightly different, indicating a small difference in composition. This suggests that the solubility limit is a somewhat 'soft' boundary, probably depending on the details of the synthesis. Clearly, Cr content does have an effect on carrier concentration and, thus, is one of the doping mechanisms for these compounds. Because the introduction of Cr also changes the oxygen content and the arrangement of oxygen atoms (as discussed above), a full understanding of how Cr substitution changes the carrier concentration is not straightforward.

The refined Cr–O distances suggest that the valence of Cr is 6 + as found previously for Sr-based Hg-1201 by EELS measurements [10]. Thus, one would expect no change in charge upon replacing a HgO_2 dumbbell with a CrO_4 tetrahedron. However, the observed variation of T_c with Cr content (Fig. 6) indicates that the carrier concentration does change. This could result from a change in the effectiveness of charge transfer from the blocking layer region to

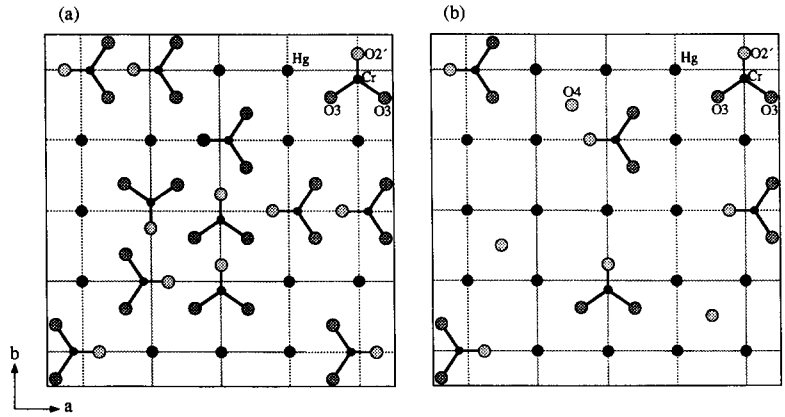

Fig. 7. Arrangement of Hg, Cr, O3 and O4 atoms in the Hg/Cr plane. Because there are two O3 atoms for each Cr atom, for a Cr content of $x = 0.5$, (a) all available oxygen-atom sites would be filled, defining the maximum allowed solubility. For lower Cr contents (b), some sites remain available for the incorporation of O4 oxygen atoms.

the CuO_2 planes or from some degree of clustering of Cr (e.g. to form Cr_2O_7 units) that would not be seen in the average structure determined by these measurements. However, the dominant cause of the change in carrier concentration is probably a change in the amount of doping from additional interstitial oxygen, O4, that is inversely correlated to the Cr content (Table 1). These O4 oxygen atoms are located at the (1/2 1/2 0) site. This is the same oxygen defect that controls carrier concentration in the pure Hg-1201 compound [12,13].

For the $Hg_{1-x}Cr_xSr_2CuO_{4+\delta}$ compounds studied previously, where $x \sim 0.5$, it was not possible to incorporate oxygen at the O4 site because all oxygen sites in the Hg/Cr plane were filled by O3 oxygen atoms associated with the Cr defects [10]. In the present compounds, where the Cr content is lower, incorporation of oxygen at the O4 site is possible and does occur. The structural features of the Hg/Cr plane for these two cases are shown in Fig. 7. As might be expected, based on these packing arguments, there is an inverse correlation between the amount of oxygen at the O4 site and the Cr content, as shown in Fig. 8. For the as-synthesized samples, n(O4) decreases from 0.139(5) for $x = 0$ to $\approx 0.06(1)$ for x near the solubility limit.

For pure $HgBa_2CuO_{4+\delta}$, T_c can be controlled by adjusting the oxygen content at the O4 site through annealing at low temperature (~ 350°C) in various oxygen partial pressures. Although there are some differences reported in the literature, for most samples, the highest T_c values are achieved by annealing in one atmosphere of oxygen and T_c can be lowered by annealing in lower oxygen partial pressures [12]. To investigate the effects of post annealing on the Cr-substituted compounds, the present samples were annealed in oxygen at 350°C for 20 h, followed by slow cooling to room temperature. Annealing experiments were also done at 150 bars oxygen and 280°C. These annealing experiments gave quite different results for the Cr-substituted samples compared to $HgBa_2CuO_{4+\delta}$. Examples of resistivity data before and after annealing are shown in Fig. 9. Note that the resistivity only measures the highest T_c fraction in the samples; therefore the observed T_c differs from the susceptibility data in Fig. 5. For the samples with $x = 0.09$ and 0.23, T_c is raised by annealing (to near the maximum T_c, 90 K), but the superconducting transition is seen in combination with increased normal-state resistivity and/or insulating behavior. For the two samples with higher Cr contents (not shown), there is no superconductivity after annealing. Insulat-

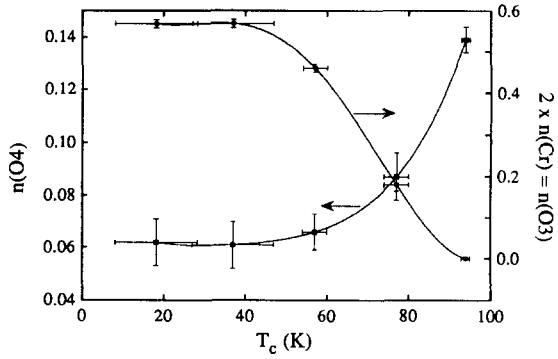

Fig. 8. Refined O3 and O4 oxygen contents vs. T_c for as synthesized samples [note the refinement constraint n(O3) = 2× n(Cr)]. There is an inverse correlation between O4 and O3 site occupancies, because of competition for the same space in the structure.

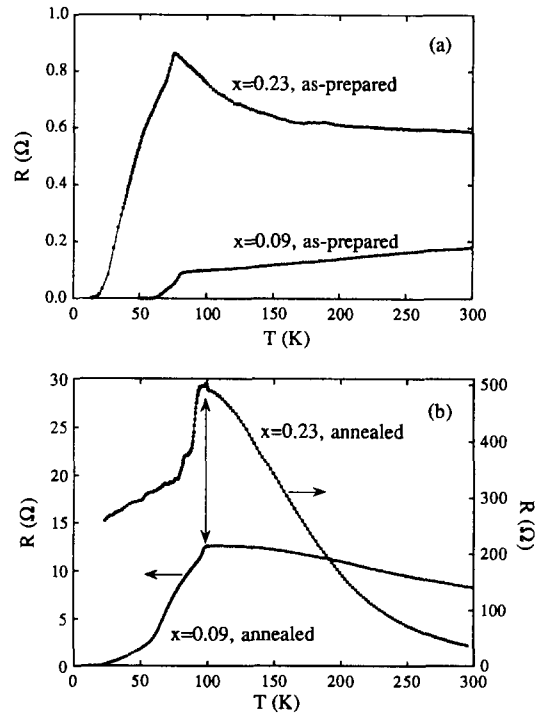

Fig. 9. Resistance measurements for the $x = 0.09$ and $x = 0.23$ samples, (a) as-synthesized and (b) after annealing in 150 bar oxygen at 280°C.

ing behavior is observed. These observations suggest that the samples phase separate upon annealing, with one of the phases being a composition with near-zero Cr content, and thus, T_c near 90 K, and the other phase being an insulating compound (as a result of high Cr content or decomposition to other compounds). For the sample with $x = 0.09$, a two-phase Rietveld refinement of data taken after annealing confirms this hypothesis. The refined O4 oxygen content for the superconducting phase was ~ 0.07, consistent with the observation of superconductivity with $T_c = 90$ K. For the other compositions, the amount of superconducting phase after annealing is too small to perform two-phase refinements.

The double superconducting transitions observed in the as-synthesized $x = 0.3$ and $x = 0.4$ samples suggest that the early stages of this phase separation affect their properties (as-synthesized). This may occur during cooling from the synthesis temperature and might be prevented by quenching, although this idea was not tested.

We conclude from these observations that the as-prepared samples are metastable. Cr can be incorporated into $HgBa_2CuO_{4+\delta}$ at high temperature under the synthesis conditions, but is apparently not soluble at the low temperatures used for oxygen annealing. However, the Cr diffusion at low temperatures limits the rate of the decomposition. Thus, even though oxygen can be incorporated at the O4 site and controls the carrier concentration, oxygen annealing at low temperature cannot be used as a technique to adjust the T_c of Cr-substituted samples.

5. Conclusions

In summary, Cr can be substituted for Hg to form the series of compounds $Hg_{1-x}Cr_xBa_2CuO_{4+\delta}$ by preparing the appropriate precursors in the correct sequence. The Cr solubility extends from $x = 0$ to about $x = 0.27$ for this synthesis procedure. When Cr substitutes at the Hg site, apical oxygen atoms are moved (O2 moves to O2′) and extra oxygen atoms (O3) are incorporated to achieve tetrahedral coordination of four oxygen atoms around each Cr atom. Because the upper limit for the solubility of Cr is less than the maximum allowed solubility of $x = 0.5$ (which is achieved in the similar $Hg_{1-x}Cr_xSr_2CuO_{4+\delta}$ compounds), [10] there are additional oxygen sites in the Hg/Cr plane (O4) that control the T_c. However, low-temperature oxygen annealing, to adjust the oxygen content in these O4 sites, cannot be used as a tool for controlling the T_c because the $Hg_{1-x}Cr_xBa_2CuO_{4+\delta}$ samples are metastable with respect to Cr content at these temperatures. Annealing results in phase separation and, eventually, decomposition and superconductivity is irreversibly destroyed.

Acknowledgements

We thank Simine Short for her help with neutron data collection. This work was supported by the US Department of Energy, Division of Basic Energy Science — Materials Sciences, under contract No. W-31-109-ENG-38 (J.D.J., D.G.H.) and by the National Science Foundation, Office of Science and Technology Centers, under grant No. DMR 91-20000 (O.C., B.G.S., B.D., H.Z., L.D.M.).

References

[1] D. Pelloquin, M. Hervieu, C. Michel, G. Van Tendeloo, A. Maignan, B. Raveau, Physica C 216 (1994) 257.
[2] S. Hahakura, J. Shimoyama, O. Shiino, K. Kishio, Physica C 233 (1994) 1.
[3] J. Shimoyama, S. Hahakura, R. Kobayashi, K. Kitazawa, K. Yamafuji, K. Kishio, Physica C 235–240 (1994) 2795.
[4] O. Chmaissem, Z.Z. Sheng, Physica C 242 (1995) 23.
[5] O. Chmaissem, Z.Z. Sheng, Z. Phys. B-Condens. Matter 99 (1996) 179.
[6] A. Maignan, D. Pelloquin, S. Malo, C. Michel, M. Hervieu, B. Raveau, Physica C 243 (1995) 233.
[7] P. Bordet, S. Le Floch, J.J. Capponi, C. Chaillout, M.F. Gorius, M. Marezio, J.L. Tholence, P.G. Radaelli, Physica C 262 (1996) 151.
[8] J. Shimoyama, K. Kishio, S. Hahakura, K. Kitazawa, K. Yamaura, Z. Hiroi, M. Takano, in: K. Yamafuji, T. Morishita (Eds.), Advances in Superconductivity VII, Springer-Verlag, Tokyo, 1995, pp. 287–290.
[9] J. Shimoyama, S. Hahakura, K. Kitazawa, Y. Yamafuji, K. Kishio, Physica C 224 (1994) 1.
[10] O. Chmaissem, D.N. Argyriou, D.G. Hinks, J.D. Jorgensen, B.G. Storey, H. Zhang, L.D. Marks, Y.Y. Wang, V.P. Dravid, B. Dabrowski, Phys. Rev. B 52 (21) (1995) 15636.
[11] O. Chmaissem, J.D. Jorgensen, K. Yamaura, Z. Hiroi, M. Takano, J. Shimoyama, K. Kishio, Phys. Rev. B. 53 (21) (1996) 14647.

[12] J.L. Wagner, P.G. Radaelli, D.G. Hinks, J.D. Jorgensen, J.F. Mitchell, B. Dabrowski, G.S. Knapp, M.A. Beno, Physica C 210 (1993) 447.
[13] O. Chmaissem, Q. Huang, A. Santoro, S.N. Putilin, M. Marezio, Physica C 212 (1993) 259.
[14] P.G. Radaelli, J.L. Wagner, B.A. Hunter, M.A. Beno, G.S. Knapp, J.D. Jorgensen, D.G. Hinks, Physica C 216 (1993) 29.
[15] S.M. Loureiro, E.V. Antipov, J.L. Tholence, J.J. Capponi, O. Chmaissem, Q. Huang, M. Marezio, Physica C 217 (1993) 253.
[16] E.V. Antipov, J.J. Capponi, C. Chaillout, O. Chmaissem, S.M. Loureiro, M. Marezio, S.N. Putilin, A. Santoro, J.L. Tholence, Physica C 218 (1993) 348.
[17] O. Chmaissem, Q. Huang, E.V. Antipov, S.N. Putilin, M. Marezio, S.M. Loureiro, J.J. Capponi, J.L. Tholence, A. Santoro, Physica C 217 (1993) 265.
[18] J.L. Wagner, B.A. Hunter, D.G. Hinks, J.D. Jorgensen, Phys. Rev. B 51 (21) (1995) 15407.
[19] Q. Huang, O. Chmaissem, C. Chaillout, J.J. Capponi, J.L. Tholence, M. Marezio, A. Santoro, Physica C 227 (1994) 1.
[20] J.D. Jorgensen, J. Faber Jr., J.M. Carpenter, R.K. Crawford, J.R. Haumann, R.L. Hitterman, R. Kleb, G.E. Ostrowski, F.J. Rotella, T.G. Worlton, J. Appl. Cryst. 22 (1989) 321.
[21] A.C. Larson, R.B. VonDreele, General Structure Analysis System, University of California, 1985–1990.